J. Fluid Mech. (1966), *vol.* 25, *part* 1, *pp.* 97–120
Printed in Great Britain

Results of an attempt to generate a homogeneous turbulent shear flow

By W. G. ROSE†
Department of Mechanics, The Johns Hopkins University

(Received 20 August 1965)

An approximately homogeneous turbulent shear flow is generated in an open-return wind tunnel test-section by a plane parallel-rod grid of uniform rod diameter and non-uniform rod spacing. The grid design is based upon an analysis by Owen & Zienkiewicz (1957). Hot-wire measurements taken in this flow include mean velocities, component turbulence intensities, shear and two-point space correlations, and energy spectra. In addition, microscales, obtained both from instantaneous time derivatives of the hot-wire signal and from two-point space correlations, and integral scales, calculated both from correlations and energy spectra, are reported.

Based upon these results, it is concluded that, far enough away from the grid and the test-section wall boundary layers:
(1) The turbulence intensities are maintained at uniform values by the nearly constant mean shear.
(2) The turbulent shear stress approaches an asymptotic value.
(3) Measured two-point space correlation coefficients and one-dimensional energy spectra attain self-preserving forms.
(4) When distance downstream of the grid is measured in terms of the number of 'local' grid rod spacings, (see discussion of microscales obtained from time derivatives), the Taylor microscale defined by the correlation coefficient $R_{uu}(r_X, 0, 0)$ grows linearly with this 'effective' distance over most of the region measured.
(5) The limited number of integral scale determinations and experimental uncertainty allow only the statements that the magnitude of the longitudinal scale is roughly one-eighth the lateral dimension of the square test-section and tends to increase slightly with 'effective' distance from the grid.
(6) The lateral integral scales are approximately one-half the longitudinal scales and also increases with distance from the grid.
(7) The integral scale which characterizes the size of the eddy primarily responsible for momentum transfer is roughly one-tenth the test-section lateral dimension (measured at one point only).

1. Introduction

An important and recognized consequence of a statistical description of turbulent shear flow is the appearance of the Reynolds stresses in the equations of mean motion. This fact results in an indeterminate system of governing equations. In effect, resolution of the indeterminacy requires additional information

† Now at the Department of Aerospace Engineering, University of Virginia.

concerning the relationship between the mean and fluctuating velocity fields. Townsend (1956) points out that all theories of shear flow '...differ from one another in making more or less plausible assumptions about the relation of the mean flow to the turbulence'.

The most commonly exploited theories are those resulting from the concept of exchange coefficient, or 'eddy' viscosity, introduced by Boussinesq (1877), and those based upon mixing-length theory developed by Taylor (1915) and independently by Prandtl (1925). Hinze (1959) discusses the distinguishing details of these theories. Townsend (1956) and Corrsin (1957) examine their limitations in the light of current understanding of shear flow. Briefly summarized, they conclude that neither mixing-length nor exchange-coefficient concepts are correct in principle; however, in the case of 'free shear flows', they do give fairly reliable predictions for the mean flow.

The need for a deeper understanding of turbulent shear flow, which is beyond the scope of mixing length or exchange coefficient theories, leads naturally to a search for 'simple' shear flows. Ordinary shear flows (channel, boundary layer, wake, and jet) are complicated by the proximity of boundaries (Corrsin 1957). In effect, their presence is communicated to each point of an ordinary flow by the big eddies which are predominantly responsible for momentum transport and interact directly with the mean motion. As this interaction of fluctuating and mean motions is the essence of the turbulent shear flow problem, boundary proximity complicates the problem in ordinary flows.

The desire to eliminate, or at least suppress, the effects of boundary proximity motivates, to some extent, consideration of the simplest conceivable turbulent shear flow, viz. a homogeneous turbulence sustained by a uniform mean shear. Ideally, homogeneity requires an infinite space. In practice, it may be realized, approximately, in a turbulent field, provided the scale of the big eddies is small compared with the distance between boundaries confining the flow.

Since its introduction by von Kármán (1937), the concept of homogeneous turbulence in a shear flow has been the subject of numerous analyses. Reis (1952), Burgers & Mitchner (1953), and Craya (1958) have examined its consequences to deduce equations for the correlations and energy spectra. Townsend (1956) applies it extensively in his study of turbulent shear flow. He points out the similarity between the mean velocity field in the neighbourhood of a point in ordinary shear flows with that in a uniform shear flow. This local motion may be decomposed into a rotation and a plane strain. In the case of the ordinary flows, it is an approximate representation.

Experiments by Townsend (1954) and Traugott (1958) investigate the turbulence associated with mean motions that, in a sense, bracket that of ordinary and uniform shear flows. Townsend's distorting duct flow is '...almost irrotational and the local motion is a pure strain.' Traugott's is one with '...uniform mean vorticity (rotational) but with no mean rate of strain'.

More recently Deissler (1961) calculated the turbulence spectra for a non-stationary homogeneous shear flow assuming low turbulence Reynolds numbers. Fox (1964) complements Deissler's results by calculating components of the velocity correlation not included in Deissler's work.

Corrsin (1963) considers the problem of actually generating a homogeneous shear flow. In reference to a grid generator, he points out: 'Although this question has yet to be explored, it appears that we have sufficient parameters available to recommend an attempt.... The flow-grid system parameters at our disposal are the following distributions: (*a*) upstream velocity, (*b*) grid rod diameter, (*c*) grid rod spacing and (*d*) local slope of the grid.' In addition, he cautions: 'It must be noted that such a homogeneous turbulent shear flow, even if generated in the laboratory, might not remain in equilibrium. There is considerable empirical evidence that the momentum carrying eddies in fully developed shear flows are not small relative to gross shear zone width (Corrsin 1957). Hence, a grid-generated homogeneous shear flow might simply develop corresponding large eddies.'

It should be mentioned that Reis (1952) extended Batchelor's (1949) theorem on the permanence of big eddies to include non-stationary homogeneous shear flow. Batchelor & Proudman (1956) have since shown that the required analyticity at zero wave-number does not hold for constant density flows. Although this invalidates the exact constancy of the biggest eddies, simple dimensional arguments show that they change relatively slowly;† Batchelor & Stewart (1950) demonstrated this in turbulence generated by a uniform grid.

In the usual grid-generated homogeneous wind tunnel turbulence, the big eddies are roughly comparable in size to grid mesh. Consequently, it is expected that the size of the big eddies in a wind tunnel shear flow will be comparable, initially, to the scale characterizing the geometry of the generating device. Hopefully, by design, it will be possible to keep this scale uniform and small compared with the test-section dimensions. Reis's results indicate that during the developing stage the small eddies decay, while the large ones persist. If, and this is the crux of the matter, a stationary state is reached, the scale of the big eddies will be that introduced by the generating device.

This paper presents the results of an attempt to generate an approximation to a homogeneous turbulent shear flow. Although the flow is conceptually simple, it retains sufficient complexity that the results of this initial exploratory investigation do not adequately answer all relevant questions.

2. Apparatus

Grid design

The essential characteristic of the grid used in this attempt is its solidity distribution (figure 1), which is determined by two considerations; viz. it must generate as uniform a mean-shear and turbulent field as is possible.

A uniform mean-shear is obtained by a grid design based upon the results of an analysis by Owen & Zienkiewicz (1957).‡ Non-uniformity of the grid-

† See, for example, Comte-Bellot & Corrsin (1965).

‡ This analysis is based upon results obtained by Taylor & Batchelor (1949) for the refraction of mean velocity incident at some angle to a fine mesh wire screen. A more recent analysis by McCarthy (1964) extends that of Owen & Zienkiewicz by solving the equations of motion 'without placing restrictions on the magnitude of variation of resistance across the grid'. This ignores grid-flow instability and consequent turbulence inhomogeneities referred to in the above discussion.

generated turbulent field is minimized by limiting the maximum solidity to 0·40. This avoids instabilities and resulting non-uniformities associated with larger values of solidity (figure 2), also Corrsin (1963). It should be noted that this restriction on maximum solidity limits the attainable maximum mean-shear and, consequently, the usefulness of a grid-produced flow as a tool for further investigation of more intensely sheared turbulent flow.

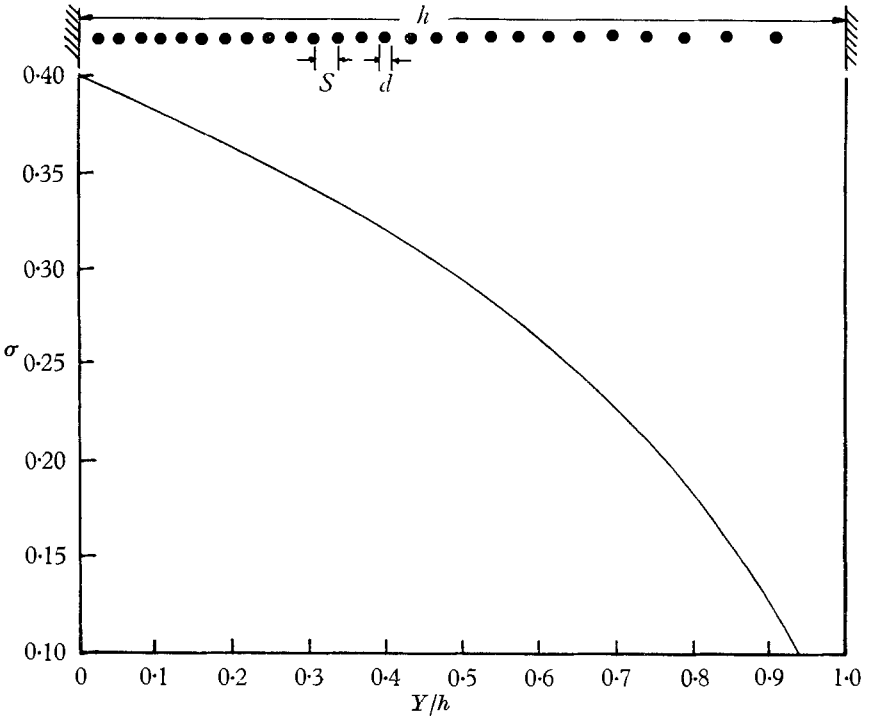

FIGURE 1. Grid solidity distribution, based on the analysis of Owen & Zienkiewicz (1957).

$$\frac{\sigma}{(1-\sigma)^2} = K_0\left[1-\frac{2h\lambda}{U_0}\left\{\frac{1}{K_0}+\frac{1}{1+a}\right\}\left\{\frac{Y}{h}-\frac{1}{2}\right\}\right],$$

where $\sigma = d/S$, d is the rod diameter $= \frac{1}{8}$ in., S is the centre-line spacing,

$$K_0 = (P_0-P_1)/\tfrac{1}{2}\rho U_0^2, \quad a = 1{\cdot}1/\sqrt{(1+K_0)}, \quad \lambda = \partial U/\partial y.$$

Design values: $\sigma_{\max} = 0{\cdot}400$; $h\lambda/U_0 = 0{\cdot}400$; $K_0 = 0{\cdot}585$.

Test facility

An open-return wind tunnel (figure 3) of nine-to-one contraction ratio and free-stream turbulence intensity less than 0·05 % was used for the experiments. The test-section was 1 ft. on a side and extended 12 ft. downstream of the grid, which was located 2 ft. downstream of the end of the contraction. A slight divergence of the test-section walls compensated for boundary-layer growth and gave, effectively, a zero pressure gradient. The test-section discharged directly into the room, so the mean static pressure equalled the ambient level.

Instrumentation

A linearized two-channel, constant-temperature hot-wire system (Hubbard 1957) was used in these tests. The modified frequency response characteristics of the R.M.S. Analyser, and differentiating circuit of this system are shown in

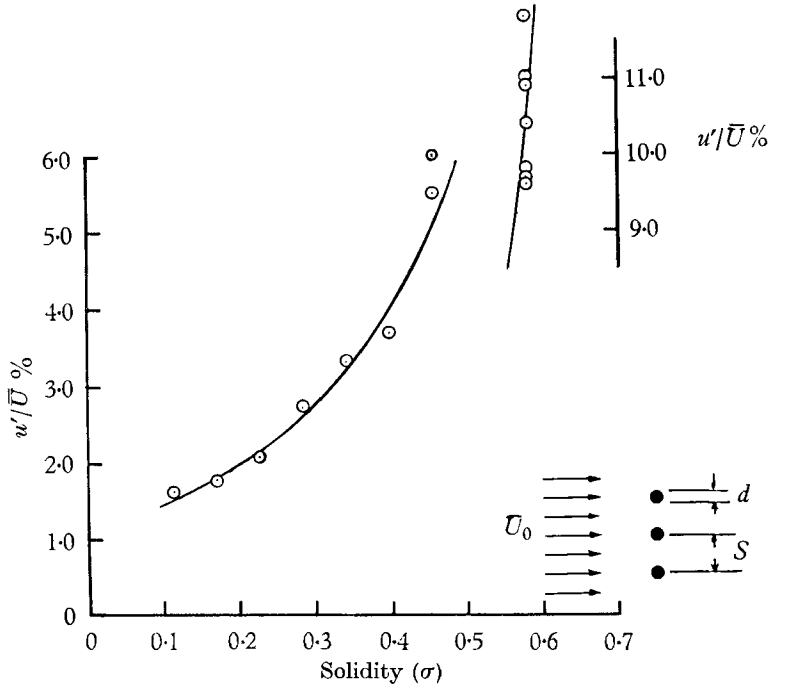

FIGURE 2. Dependence of turbulence intensity on solidity of a uniform parallel round-rod grid. $X/S = 38{\cdot}0$; $R = \bar{U}_0 S/\nu = 2 \times 10^4$; $(u'/\bar{U})_0 = 0{\cdot}25\,\%$; $\sigma = d/S$.

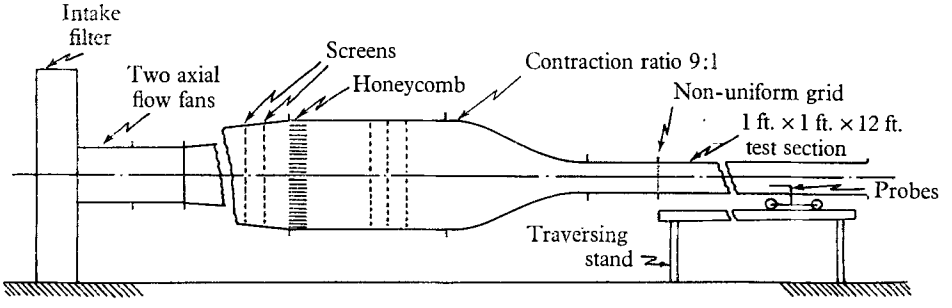

FIGURE 3. Schematic of wind-tunnel facility. Open-return wind tunnel. 1 ft. × 1 ft. × 12 ft. test section, 0·05 % free-stream turbulence level.

figures 4 and 5. The sensing elements were fabricated from $1{\cdot}5 \times 10^{-4}$ in. tungsten wire approximately 0·75 mm long and operated at an overheat ratio of 0·8. Drift of wire calibrations was virtually eliminated by passing the air supply through filters composed of fibres with diameters of the order of a micron (Collis 1952; Pasceri & Friedlander 1960) and maintaining the room where the tunnel was located at a constant temperature to within a fraction of a degree.

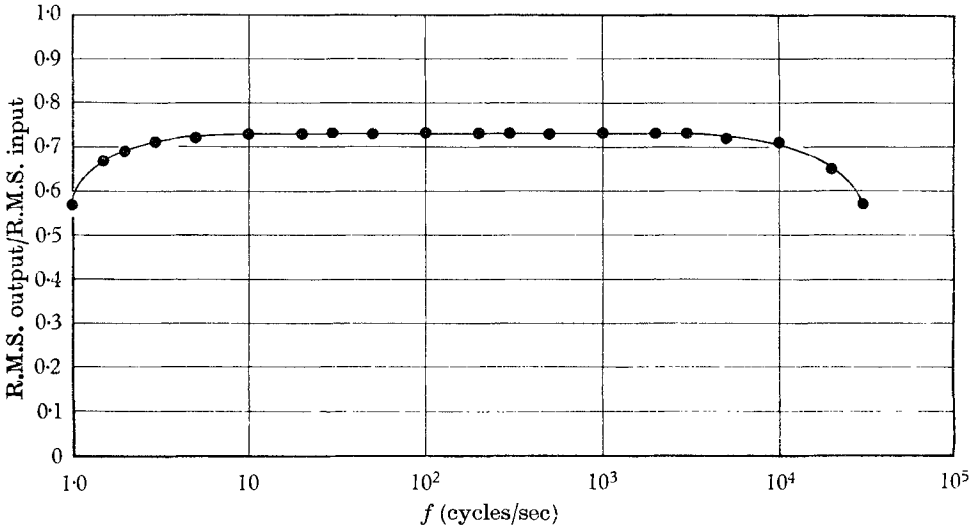

FIGURE 4. Modified frequency response of R.M.S. Analyser.

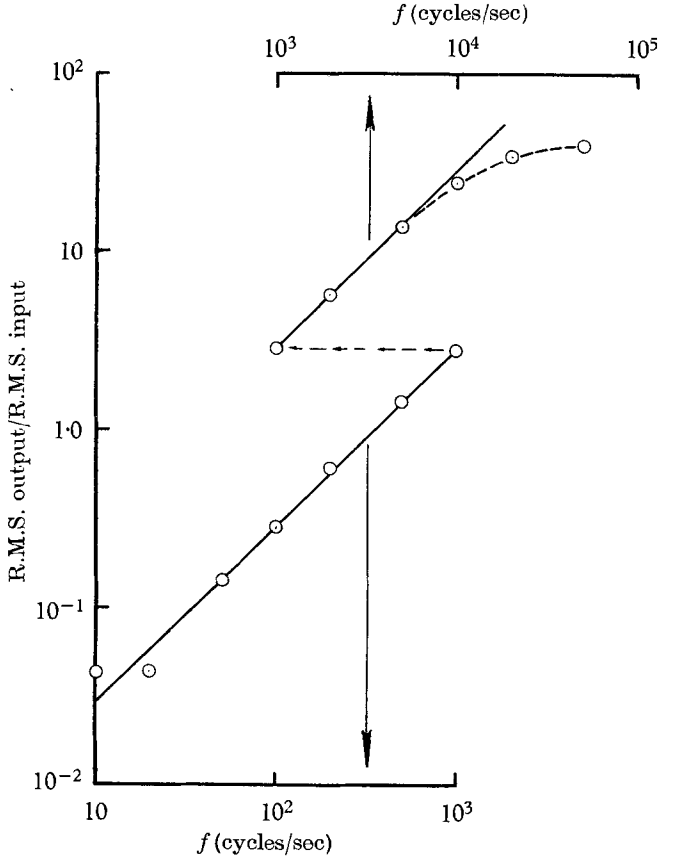

FIGURE 5. Modified frequency response of differentiating circuit.

Equipment used in the measurement of energy spectra is described by Gibson (1963). All time averaging of the signals was done by analogue integration (Rose 1962).

3. Results

Close to the grid

It is expected that the flow just downstream of the grid (figure 6) will reflect its non-uniform origin, and it is of interest to note exactly the evidence for this non-uniformity. Lateral distributions of mean velocity $\overline{U}/\overline{U}_c$, intensities $u'/\overline{U}_c$ and $v'/\overline{U}_c$, and shear correlation $\overline{uv}/\overline{U}_c^2$ taken along the direction of the mean-velocity gradient at a distance X/h downstream of the grid plane equal to 1·33 are shown in figure 7.

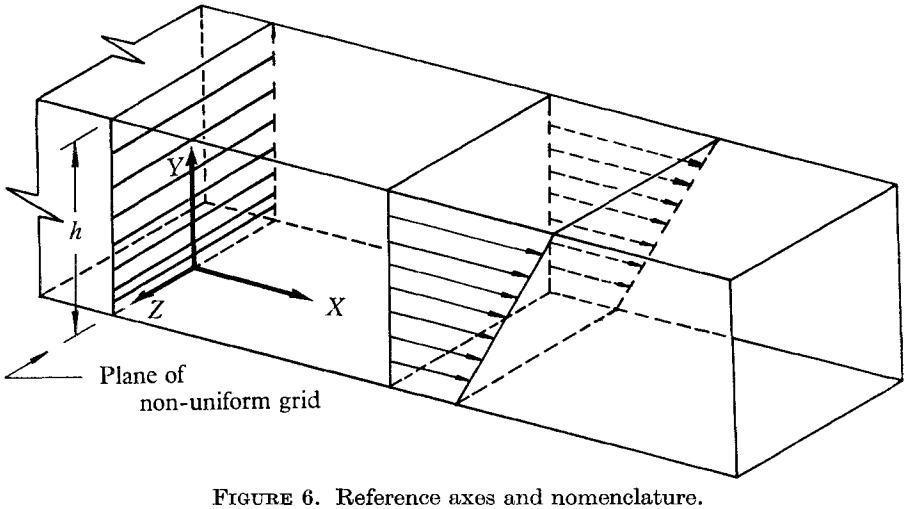

FIGURE 6. Reference axes and nomenclature.

Co-ordinate	Mean component velocity	R.M.S. value fluctuating component velocity
X	$\overline{U} = \overline{U}(Y)$	u'
Y	$\overline{V} = 0$	v'
Z	$\overline{W} = 0$	w'

The mean-velocity profile is compared with a solid straight line which represents the faired slope of the profile measured farther downstream at X/h equal to 7·89. This average slope corresponds to a value of non-dimensionalized mean shear $h/\overline{U}_c \partial\overline{U}/\partial Y$ equal to 0·27. Scatter of the measured points about this average slope, over the range $0{\cdot}1 \leqslant Y/h \leqslant 0{\cdot}9$, is less than $\pm 2{\cdot}0\,\%$. Consequently, the grid generates a nearly uniform mean shear within one-and-one-third grid spans downstream of its location.

Uniformity of the turbulent field is less well established at this downstream location. This is indicated by the straight lines connecting points of the shear correlation, $\overline{uv}/\overline{U}_c^2$. Although the intensity distributions, $u'/\overline{U}_c$ and $v'/\overline{U}_c$, are quite uniform, uniformity of the shear correlation appears to be a more difficult

criterion to satisfy. This quantity too must be constant for a homogeneous turbulence to exist. The fact that the turbulence production is proportional to the product of the shear correlation and mean strain rate could lead to growth of the non-uniformity. Downstream data indicate that this is not the case.

It should be remarked that the increase in the u-intensity in the region Y/h approaching unity is consistent with the fact that fluid in this region has travelled a fewer number of 'local' grid rod-spacings.

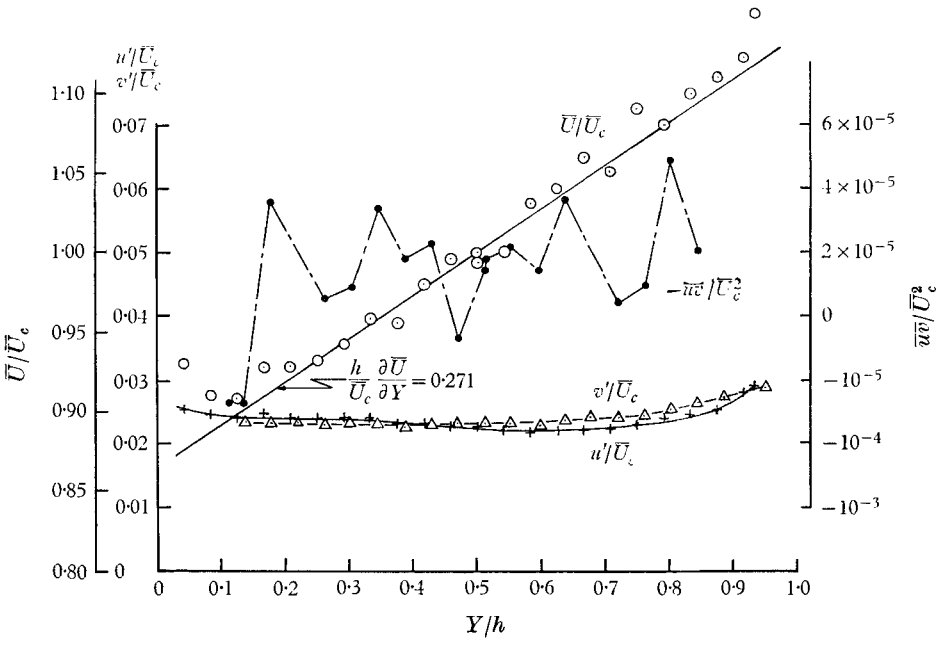

FIGURE 7. Lateral distributions: $X/h = 1{\cdot}33$, $Z/h = 0$.

Farther downstream from the grid

Evolution of the motion as the fluid moves away from the grid is shown partially by figures 8–13. Test-section centre-line distributions (figure 8) show the decay of the turbulent intensities from their levels close to the grid to uniform values which are, presumably, characteristic of the uniform mean-shear magnitude sustaining the turbulence. It is not surprising that the u-component intensity attains its asymptotic value upstream of the location where the v- and w-components attain their asymptotic values. In rectilinear and nearly rectilinear flow, conversion of mean-flow kinetic energy to turbulent kinetic energy occurs directly through the u-component (Corrsin 1957). However, it is not obvious just how this turbulent energy is to be partitioned among the three fluctuating components. From the present results, it is calculated that roughly one-half the total kinetic energy of the fluctuations is divided equally between the v- and w-components. This ignores the slight difference between the final levels of these two components which is shown in figure 8.

Of the remaining three distributions included in figure 8, the shear correlation and correlation coefficient are the most interesting. The nearly constant value

of centre-line mean velocity provides a check on the wall adjustment compensating for boundary-layer growth. The shear correlation increases monotonically to what appears to be an asymptotic value. Approximately 25 % of this increase

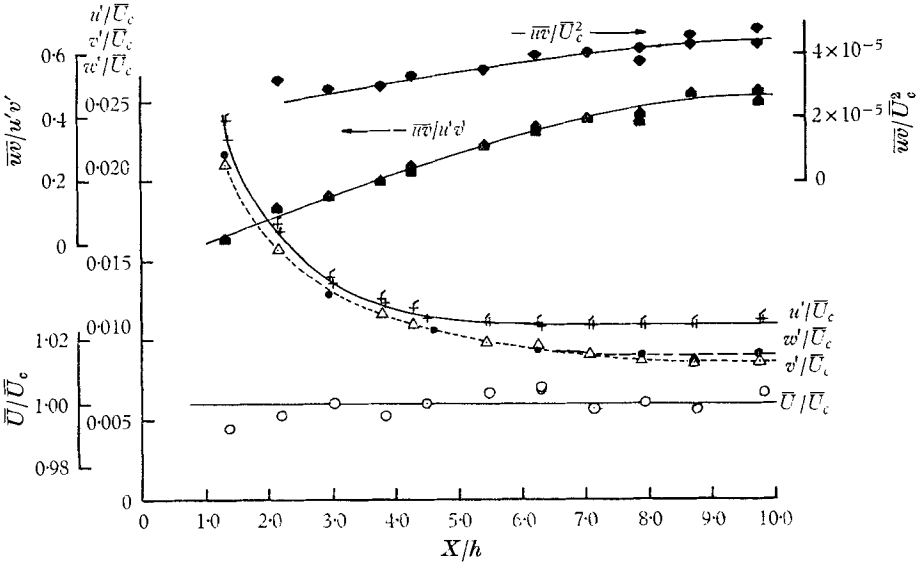

FIGURE 8. Centre-line distributions: $Y/h = 0{\cdot}5$, $Z/h = 0$. $\bar{U}_c = 50{\cdot}5$ ft./sec., $h = 12$ in.

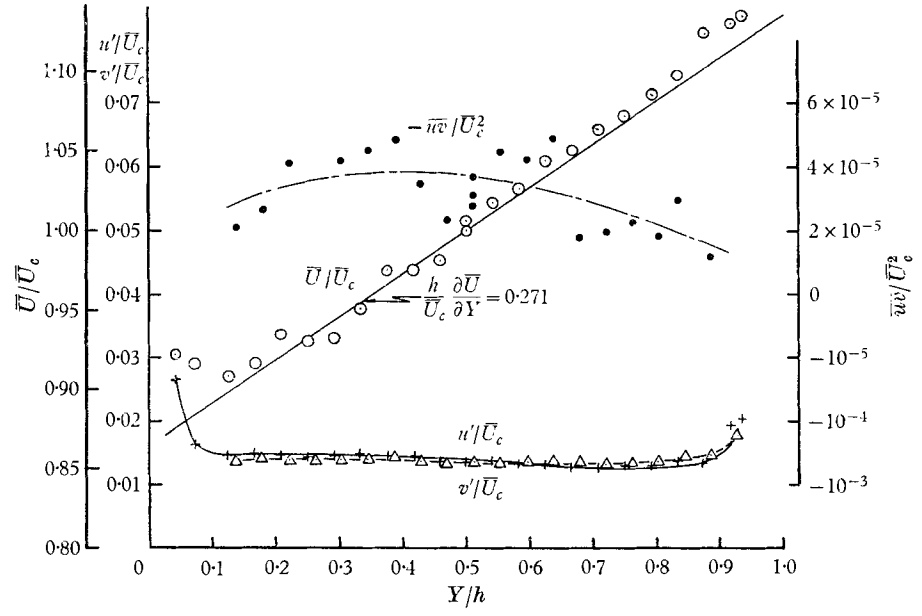

FIGURE 9. Lateral distributions: $X/h = 2{\cdot}97$, $Z/h = 0$.

occurs downstream of the location where the u-component intensity reaches its asymptotic level. The remaining point of interest is the asymptotic level of the shear correlation coefficient, 0·45, a value close to those found commonly for other shear flows.

Additional evidence, as to the manner in which the motion evolves, is presented in figures 9–13. Briefly, these results establish the following facts, excluding the region of the developing wall boundary layers, the mean-shear and the turbulence intensity components are very nearly constant throughout the field. The initial wild variation of the shear correlation is reduced considerably. Its measured value at $X/h = 9{\cdot}76$ decreases in magnitude from roughly -5×10^{-5} to

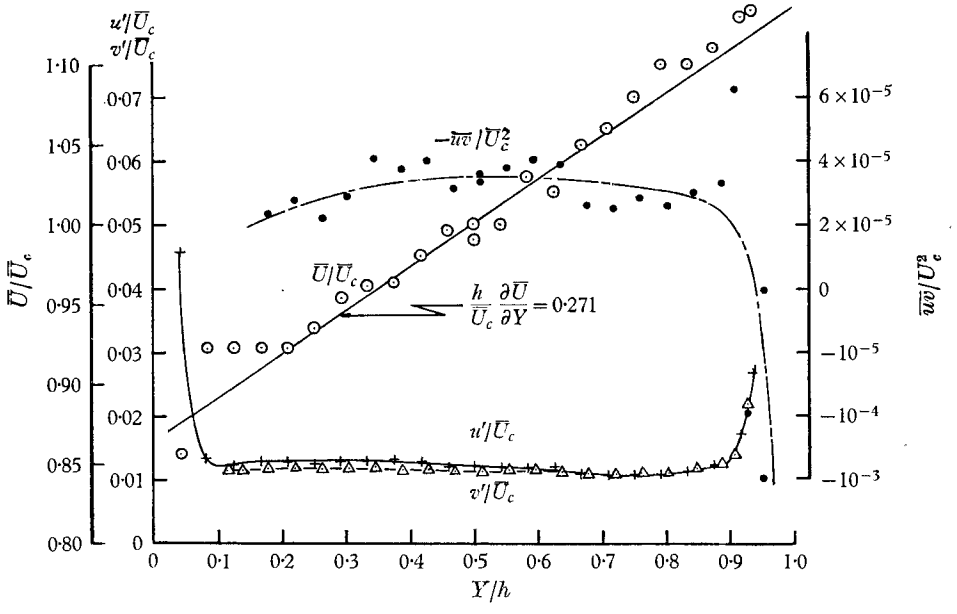

FIGURE 10. Lateral distributions: $X/h = 4{\cdot}28$, $Z/h = 0$.

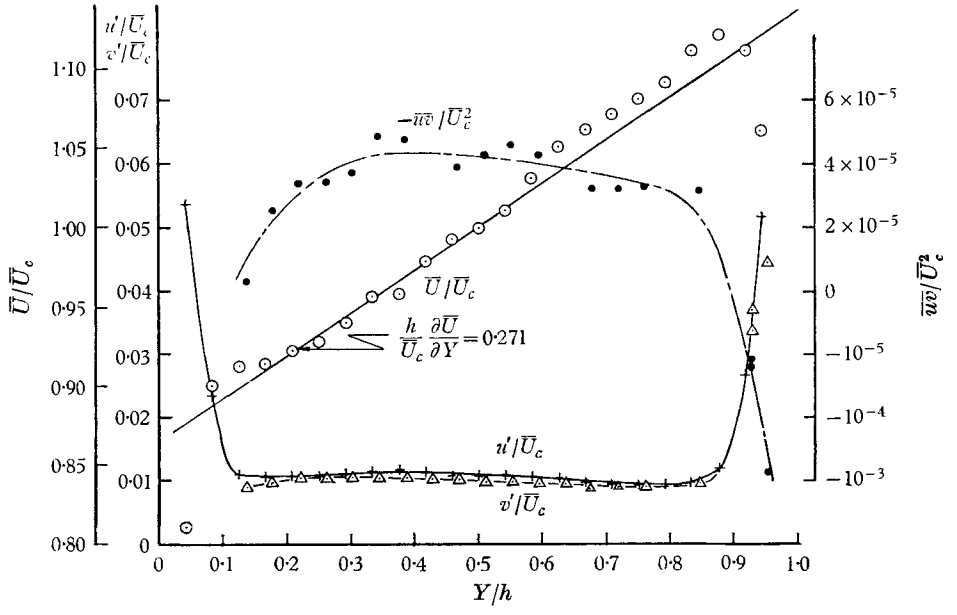

FIGURE 11. Lateral distributions: $X/h = 6{\cdot}25$, $Z/h = 0$.

-3×10^{-5} over the region $0{\cdot}4 \leqslant Y/h \leqslant 0{\cdot}8$. Two shear-correlation scales are used in these figures to give some indication as to the relative magnitude of the correlation in the region of uniform mean-shear compared with its value in the wall boundary layer. It changes by several orders-of-magnitude (figure 13). An unexplained point of interest is the development of minima in the intensity distributions along with overshoots in the mean-velocity profile. These occur close

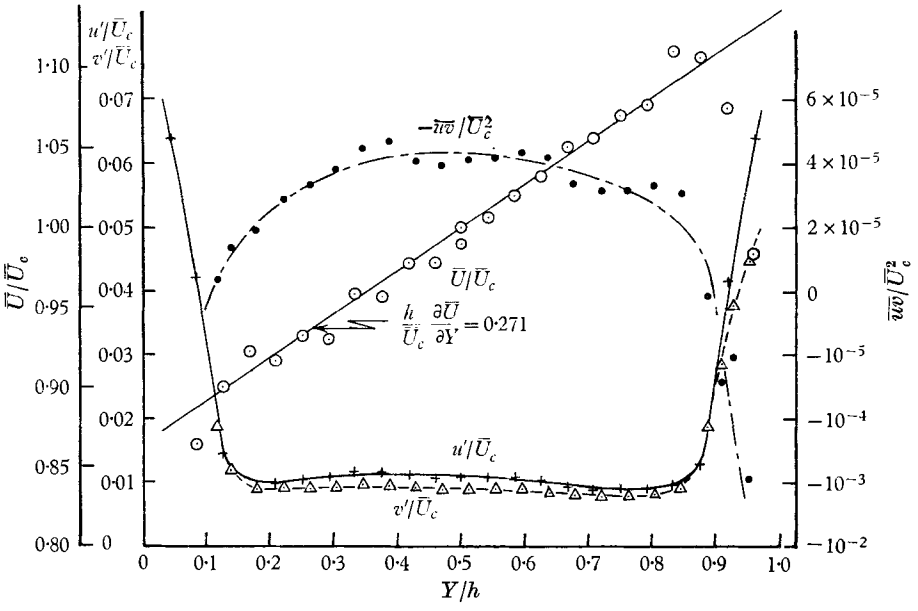

FIGURE 12. Lateral distributions: $X/h = 7{\cdot}89$, $Z/h = 0$.

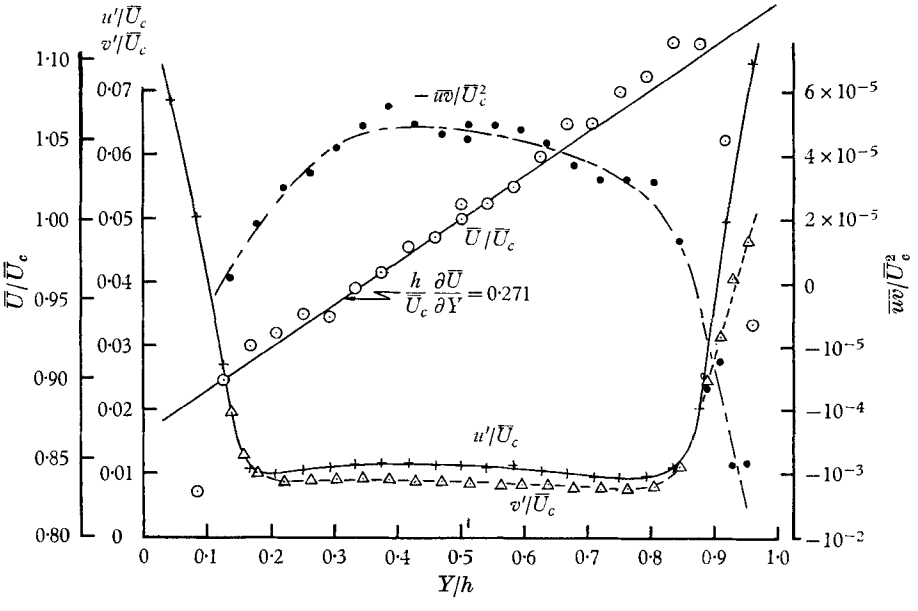

FIGURE 13. Lateral distributions: $X/h = 9{\cdot}76$, $Z/h = 0$.

to the outer 'edge' of the boundary layers (figures 11–13). Figure 14 is a composite plot of the lateral distributions of the shear-correlation coefficient. Its value is seen to develop from something on the order of $-0{\cdot}05$ close to the grid to roughly $-0{\cdot}45$ at the most downstream position.

Two-point space correlations

The central role played by velocity correlations and energy spectra in attempts at understanding the dynamics of turbulent flow motivates their measurement. Most important for present purposes are the turbulence scales which are defined in terms of the correlation and spectrum functions. Ideally, if the turbulence is to be homogeneous these scales must have uniform values throughout the flow, after it reaches an asymptotic state.

The two-point correlation coefficient of the fluctuating velocity components in the mean-flow direction, at a point specified by the position vector $\mathbf{X}$ with components X, Y, Z, and point separation given by the vector $\mathbf{r}$ with components r_X, r_Y, r_Z, is by definition

$$R_{uu}(\mathbf{X}, \mathbf{r}) = \overline{u(\mathbf{X})\, u(\mathbf{X}+\mathbf{r})}/u'^2,$$

where the overbar designates a time average value. The longitudinal Taylor microscale λ_X, is defined for convenience by the relation

$$\lambda_X^2 = 2u'^2/\overline{(\partial u/\partial X)^2}.$$

Lateral microscales λ_Y and λ_Z are given by derivatives with respect to Y and Z respectively. The longitudinal integral scale L, is defined by

$$L_X = \int_0^\infty R_{uu}(r_X, 0, 0)\, dr_X.$$

Lateral integral scales L_Y and L_Z are given by integrations, with respect to r_Y and r_Z respectively, of $R_{uu}(0, r_Y, 0)$ and $R_{uu}(0, 0, r_Z)$.

In order that the turbulence be homogeneous, the correlation coefficients must be even functions of the point separation. As a consequence, these coefficients are given approximately for sufficiently small separations by the first two terms of a Taylor series, for example, the coefficient

$$R_{uu}(r_X, 0, 0) \cong 1 - r_X^2/\lambda_X^2.$$

This functional form for the correlation coefficient suggests a convenient way of displaying the experimental results, viz. a log-log plot. Figures 15(*a*), 16(*a*), 17(*a*) and 18(*a*) have been constructed with this in mind. The straight solid line included on these plots has a slope of 2. It represents the required functional form for the correlation coefficients in the limit of small separations. The results indicate that this necessary condition for a homogeneous turbulence is satisfied by the present flow.

It should be remarked that the correlations were generated by using a sum and difference ('quarter square') technique. Consequently, the accuracy of the results when the value of the coefficient is close to unity is very poor. However, for values of $1 - R_{uu}$ close to 10^{-1} the experimental scatter is sufficiently small that

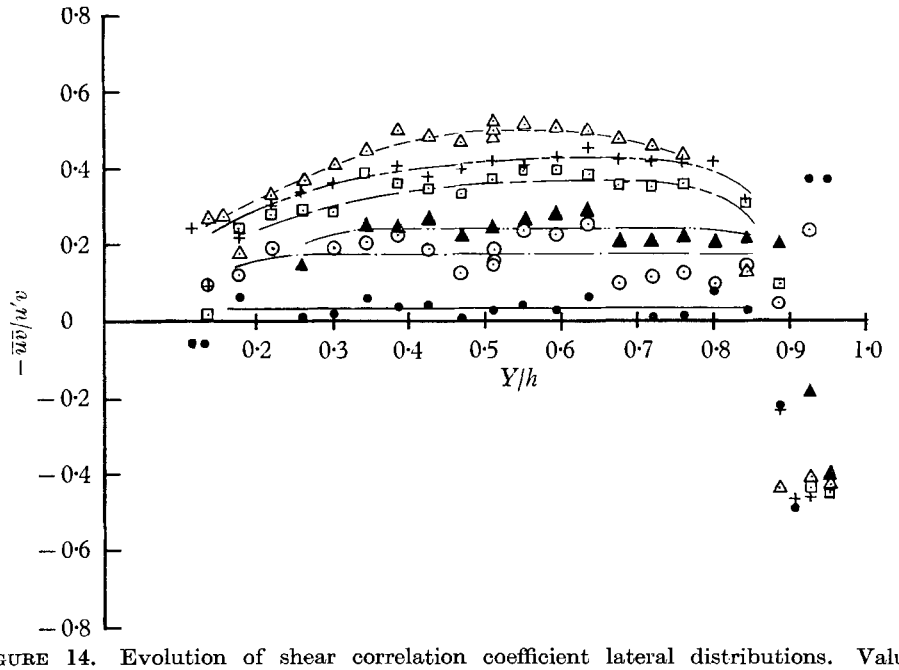

FIGURE 14. Evolution of shear correlation coefficient lateral distributions. Values of X/h: ●, ——, 1·33; ⊙, ——·——, 2·97; ▲, ——··——, 4·28; ⊡, — — —, 6·25; +, — — — —, 7·89; △, — — —, 9·76.

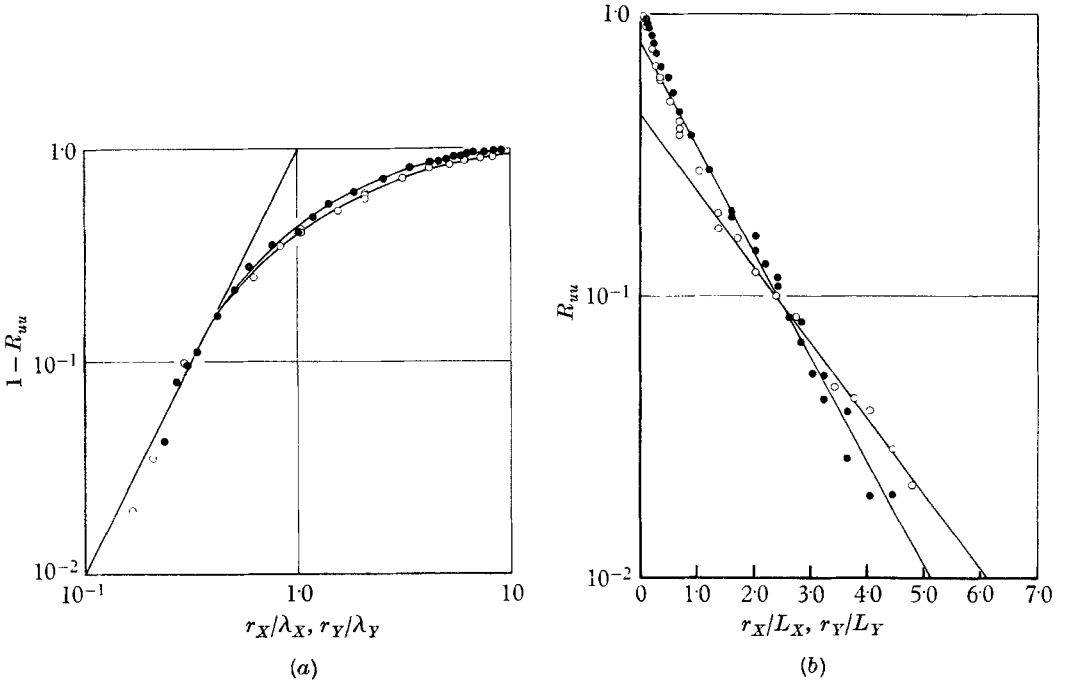

FIGURE 15. Two-point velocity correlation coefficient: $X/h = 7{\cdot}5$, $Y/h = 0{\cdot}5$, $Z/h = 0$. (*a*) Small point separations: ○, $1-R_{uu}(r_X, 0, 0)$, $\lambda_X = 0{\cdot}48$ in.; ●, $1-R_{uu}(0, r_Y, 0)$, $\lambda_Y = 0{\cdot}29$ in. (*b*) Large point separations: ⊙, $R_{uu}(r_X, 0, 0)$, $L_X = 1{\cdot}46$ in.; ●, $R_{uu}(0, r_Y, 0)$, $L_Y = 0{\cdot}62$ in.

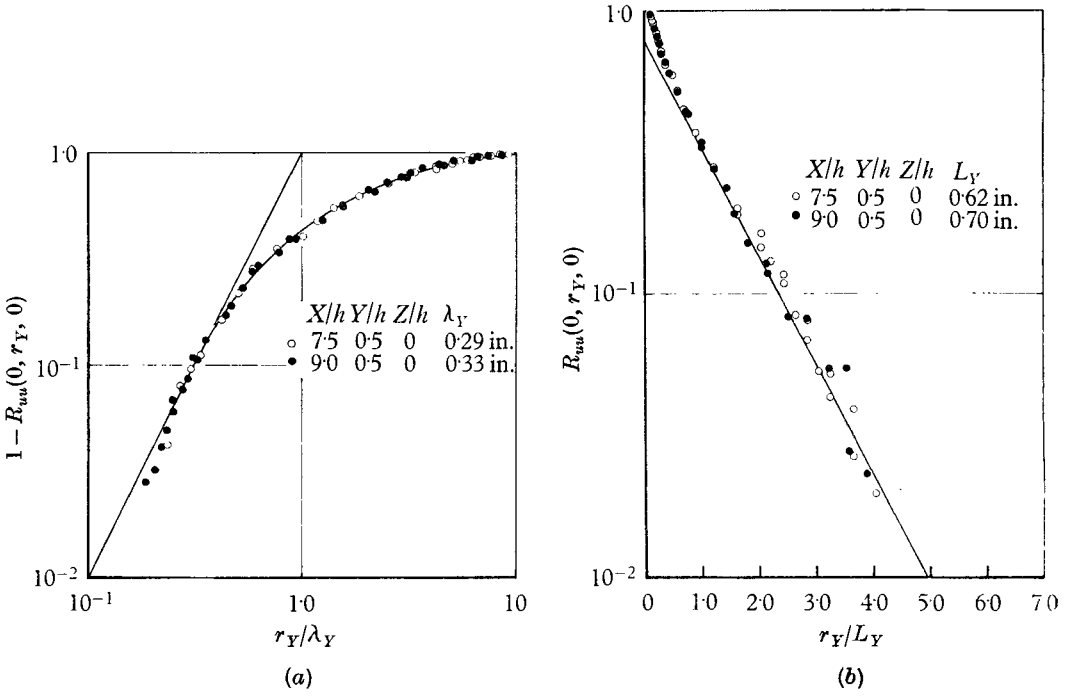

FIGURE 16. Two-point velocity correlation coefficient: (*a*) small point separations; (*b*) large point separations.

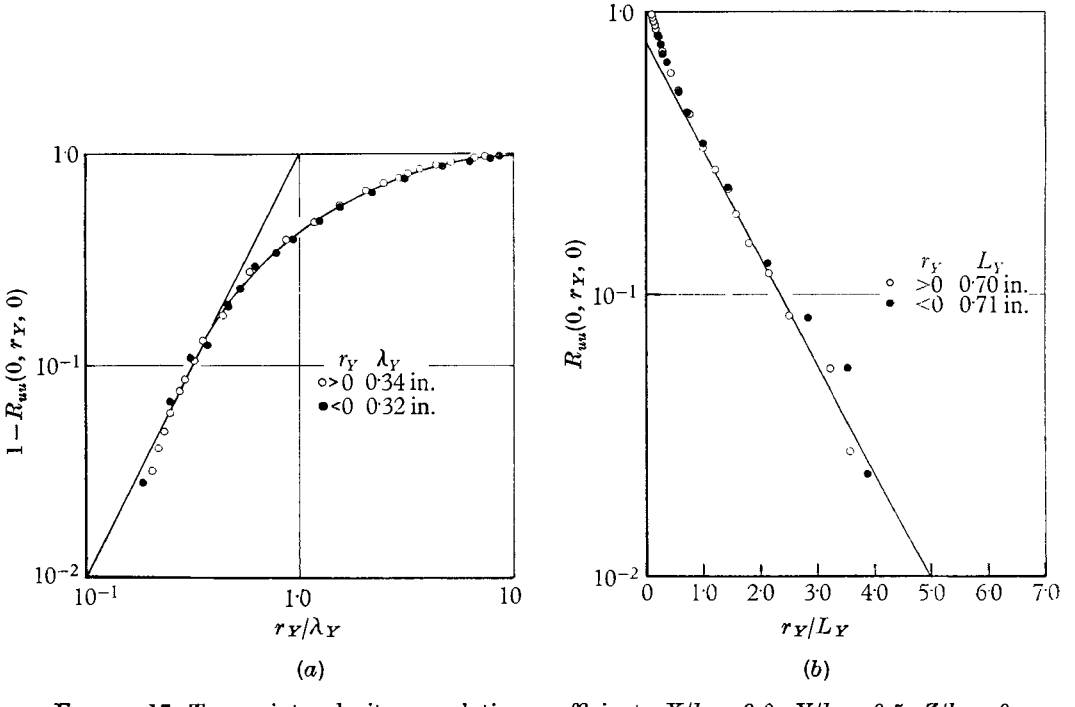

FIGURE 17. Two-point velocity correlation coefficient: $X/h = 9{\cdot}0$, $Y/h = 0{\cdot}5$, $Z/h = 0$. (*a*) Small point separations; (*b*) large point separations.

the number of points measured in this region determine the functional form of the distribution at small separations, and consequently fix the values of the microscales to within an estimated $\pm 5\,\%$.

In all the correlation measurements to be reported, except $R_{uu}(0,0,r_Z)$ and $R_{uv}(0,r_Y,0)$, the axes of the wire-sensing elements were oriented parallel to the Z-axis, i.e. normal to both the direction of the mean flow and that of the mean-velocity gradient. The length of wire-sensing element l_w used, relative to the Taylor microscale, is indicated in figure 18(*a*).

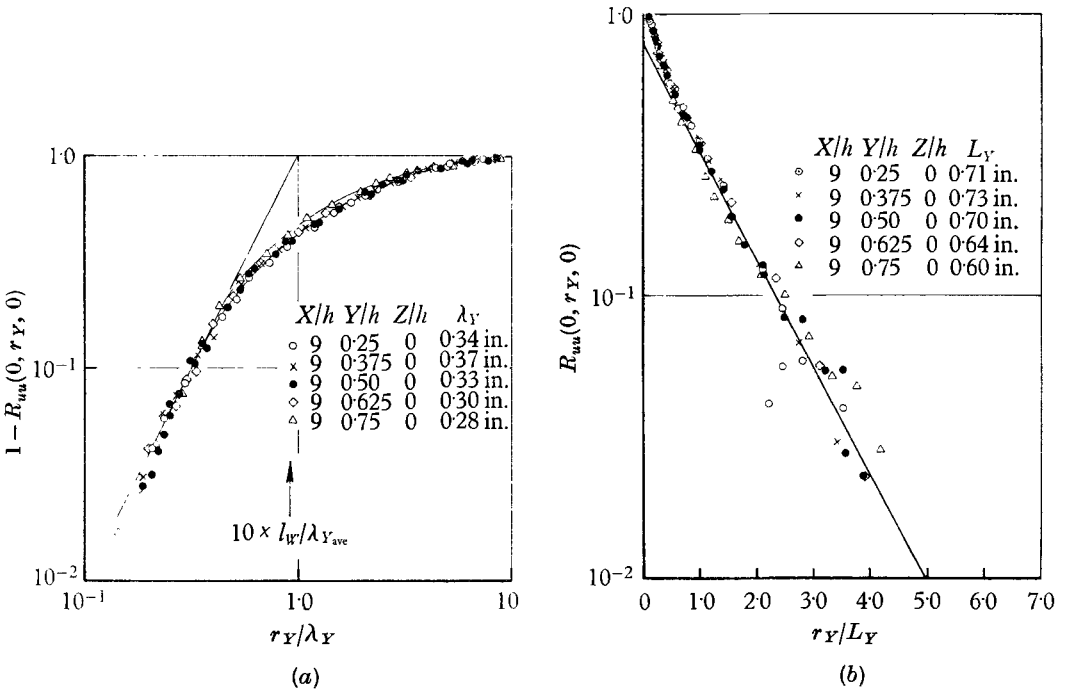

FIGURE 18. Two-point velocity correlation coefficient: (*a*) small point separations; (*b*) large point separations.

Results of measurements at large point separations (figures 15(*b*), 16(*b*), 17(*b*), 18(*b*)), are displayed best by semi-log plots. These exhibit what appears to be a characteristic feature of shear flow, viz. correlation coefficients of component fluctuations in the mean-flow direction, when the point separation is in a direction normal to that of the mean flow and along that of the mean-velocity gradient, are monotonically decreasing functions of the separation distance, as long as the two points are in a region of monotonic mean-velocity variation.† This is not true of the other lateral correlation, $R_{uu}(0,0,r_Z)$, which takes negative values at large separations (figure 19).

Within the accuracy of the sum and difference technique used to measure the correlations, at large point separations the coefficients approach zero exponen-

† This is found to hold in channel flow (Laufer 1951; Comte-Bellot 1965), wakes and boundary layers (Grant 1958), and jets (Kolpin 1964).

tially with increasing separation. The solid straight line of figures 16(*b*), 17(*b*) and 18(*b*) is the same on all three plots for convenience in making a comparison of these results. Such a comparison indicates that the distributions are very nearly similar.

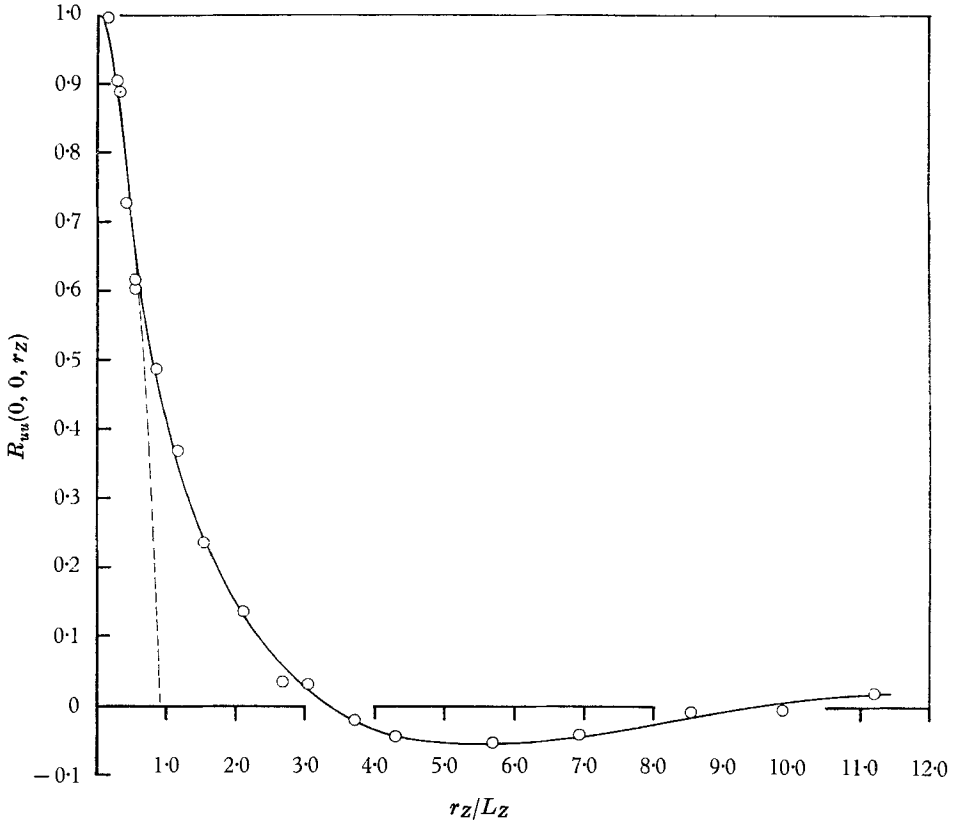

FIGURE 19. Two-point velocity correlation coefficient: point separations along direction normal to mean flow and velocity gradient. $X/h = 9{\cdot}0$, $Y/h = 0{\cdot}5$, $Z/h = 0$; $\lambda_Z = 0{\cdot}33$ in., $L_Z = 0{\cdot}36$ in.

Considerable effort was required for measuring $R_{uu}(r_X, 0, 0)$ (figures 15(*a*), 15(*b*)). Each point was obtained from a lateral traverse of the downstream wire along a constant r_X line, and extrapolation of the resulting profiles of $R_{uu}(r_X, r_Y, 0)$ to obtain a value for $R_{uu}(r_X, 0, 0)$. Only one longitudinal distribution of $R_{uu}(r_X, 0, 0)$ was attempted. It was found that an appreciable systematic error in the magnitude of $R_{uu}(r_X, 0, 0)$ results when its value is approximated by placing the wire just 'outside' the wake of the upstream wire. This is especially true for small separations in the streamwise direction where errors on the order of $-5\,\%$ would result.

A comparison of the longitudinal and lateral correlation coefficients $R_{uu}(r_X, 0, 0)$ and $R_{uu}(0, r_Y, 0)$, together with the values of their associated microscales and integral scales, is given in figures 15(*a*) and 15(*b*).

Figures 16(*a*) and 16(*b*) show the lateral correlation coefficient distributions

$R_{uu}(0, r_Y, 0)$ at two locations downstream of the grid corresponding to values of $X/h = 7{\cdot}5$ and $9{\cdot}0$. Although these distributions are similar, with no discernible systematic variations, the scales increase with distance from the grid. The microscale increases by 14 % and the integral scale by 13 %. It is estimated that the accuracy of the scale values determined from the lateral correlations is ± 5 %.

Figures 17(*a*) and 17(*b*) provide a check on homogeneity of the turbulence in the centre of the test-section. These plots of the lateral distribution of $R_{uu}(0, r_Y, 0)$ represent results obtained for point separations along the direction of increasing and decreasing mean velocity, $r_Y > 0$ and $r_Y < 0$ respectively. The two distributions are similar. The 6 % difference in the values of their microscales and the 1·4 % difference in the integral scales are not significant, in view of the accuracy of the scale values.

Figures 18(*a*) and 18(*b*) are composite plots of the coefficient distributions obtained at five locations along the mean-velocity gradient, all taken at the same distance from the grid, $X/h = 9{\cdot}0$. Excluding the results for $Y/h = 0{\cdot}75$, the distributions are similar. The distribution for $Y/h = 0{\cdot}75$ is excluded on the basis that this location is influenced by the wall boundary layer (figures 13, 14) and is effectively too close to the grid (figure 24).

Figure 19 is a rectilinear plot of the lateral correlation coefficient, $R_{uu}(0, 0, r_Z)$, obtained for point separations along a direction normal to both that of the mean flow and that of the mean-velocity gradient. Contrasted with lateral distributions along the gradient, this distribution takes on negative values at large point separations. Although the microscale values obtained for the two lateral directions are the same, the integral scale along the gradient is almost twice that normal to the gradient. This lateral distribution, $R_{uu}(0, 0, r_Z)$, was obtained with the wire axes oriented parallel to the direction of the mean-velocity gradient.

Figure 20 is a semi-log plot of the cross-correlation coefficient $R_{uv}(0, r_Y, 0)$ which is obtained from measurements at $X/h = 9{\cdot}0$. From this distribution, it is possible to define a scale which characterizes the size of eddy predominately responsible for momentum transfer and, consequently, the turbulent shear stress. Its definition is

$$L = \int_0^\infty R_{uv}(0, r_Y, 0)\, dr_Y.$$

The value of L determined from the measurements is roughly one-tenth the test-section lateral dimension.

One-dimensional energy spectra

Results obtained from measurements of the one-dimensional energy spectra are given in figures 21 and 22. The measured frequencies have been converted to wave-numbers by the relationship $K_X = 2\pi f/\overline{U}$, where f is the frequency, $\overline{U}$ the local mean velocity, and K_X the wave-number in the mean-flow direction. The independent variable is the non-dimensional product of wave-number K_X and Kolmogoroff microscale $\eta = (\nu^3/\epsilon)^{\frac{1}{4}}$, where ν is the kinematic viscosity, and ϵ the dissipation rate. The value of ϵ is obtained by equating it to the

production rate since the lateral transport terms are negligible. The production rate $-\overline{uv}\,\partial\overline{U}/\partial Y$ is calculated in turn from the results of measurements taken far from the grid. Equating the production to the dissipation is justified by the measured uniformity of the turbulence intensities.

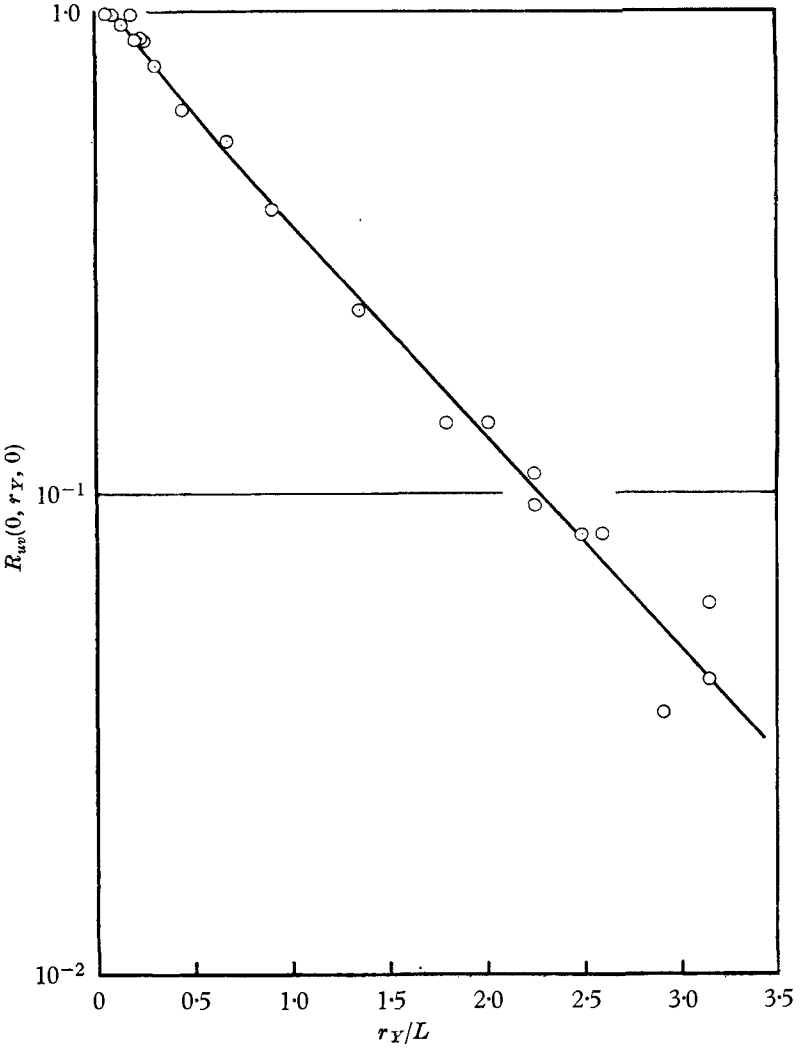

FIGURE 20. Two-point cross-correlation coefficient. $X/h = 9{\cdot}0$, $Y/h = 0{\cdot}5$, $Z/h = 0$, $L = 1{\cdot}1$ in.

Figure 21 compares spectra obtained at two downstream locations from the grid, $X/h = 7{\cdot}5$ and $9{\cdot}0$. They are not similar. There is relatively less energy in the higher wave-numbers of the spectrum at $X/h = 9{\cdot}0$. Also, the integral scale at this location is 23 % larger than that found at $X/h = 7{\cdot}5$.

Integral scales are computed from the spectra by using the relationship

$$L_X = \frac{\overline{U}}{4} E_u(0) \Big/ \int_0^\infty E_u(f)\,df,$$

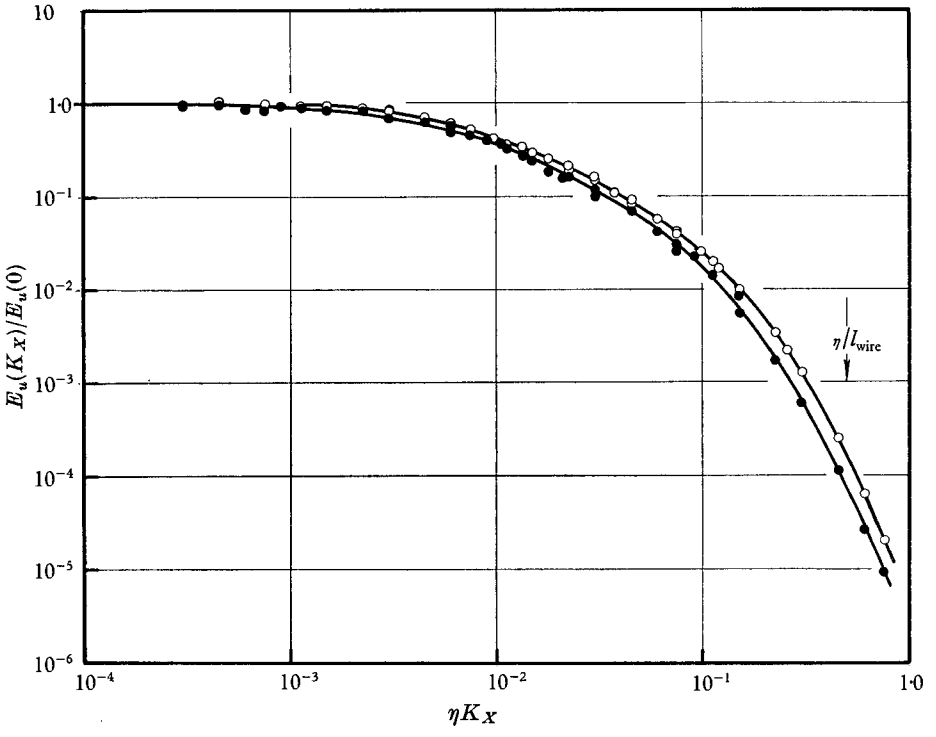

FIGURE 21. One-dimensional energy spectra.

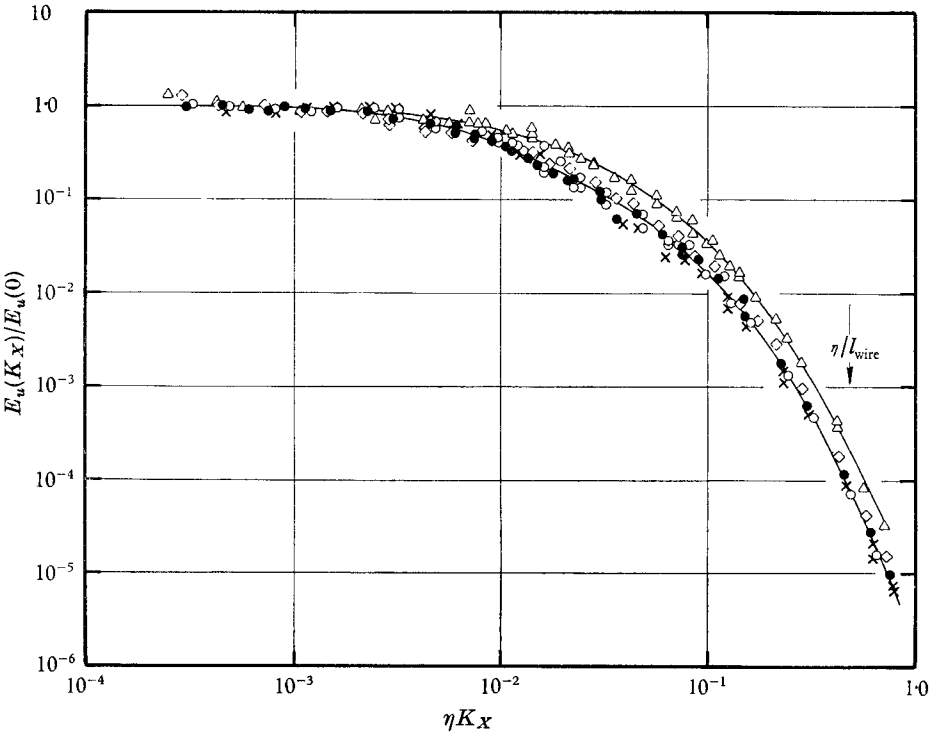

FIGURE 22. One-dimensional energy spectra.

where f is frequency in cycles per second. Definitions of integral scale in terms of correlations and spectra are equivalent, since the correlation is the Fourier cosine transform of the one-dimensional energy spectrum. Because of experimental scatter, extrapolation of the measured spectra to zero frequency, to obtain $E_u(0)$ needed in the calculation of integral scales, limits the accuracy of the scales to $\pm 10\,\%$. Figure 22 is a composite plot of the spectra corresponding to the correlations of figures 18(*a*) and 18(*b*). As in the case of the correlations, the resulting distributions are nearly similar excepting that which is influenced by the wall boundary layer $Y/h = 0{\cdot}75$. The length of the wire sensing element, l_w, relative to η, is indicated on both figures 21 and 22.

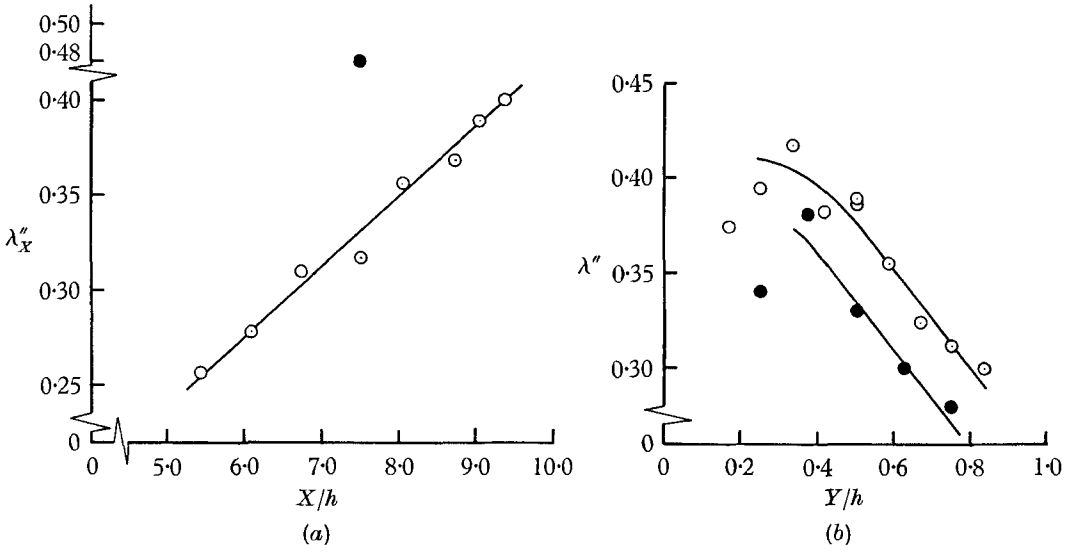

FIGURE 23. Taylor microscales: (*a*) Centre-line variation: $Y/h = 0{\cdot}5$, $Z/h = 0$. ⊙, $\overline{(\partial u/\partial t)^2}$; ●, $R_{11}(r_X, 0, 0)$. (*b*) Lateral variation: $X/h = 9{\cdot}0$, $Z/h = 0$. ⊙, λ_X, $\overline{(\partial u/\partial t)^2}$; ●, λ_Y, $R_{uu}(0, r_Y, 0)$.

Microscales obtained from time derivatives

Assuming the transformation $\partial/\partial t = \overline{U}\,\partial/\partial X$ to be applicable (Lin 1953; Lumley 1965), values of the microscale λ_X have been calculated from time derivatives of the hot-wire signal. Figures 23(*a*) and 23(*b*) present λ_X distributions obtained from traverses along the test-section centre-line and transverse to the centre-line in the direction of the mean-velocity gradient. These values of λ_X are corrected for noise, and discussed in the following section. The spatial variation of the microscale, which increases with distance from the grid and decreases, for the most part, with increasing Y/h, suggests that the turbulence retains some evidence of its grid-generated origin.

In decaying homogeneous turbulence, generated with a square-mesh round-rod grid at constant grid Reynolds number, the turbulence properties are functions of the number of mesh lengths the fluid has moved downstream of the grid.

For the non-uniform parallel round-rod grid, used to produce the shear flow, rod centre-line spacing is analogous to mesh size and provides an appropriate parameter for calculating an 'effective' distance from the grid. This has been done, in a crude way, by neglecting the boundary-layer displacement thickness and using the continuity equation to relate the downstream Y-location of fluid to its Y-location at the grid, hence, the 'local' grid rod spacing, S.

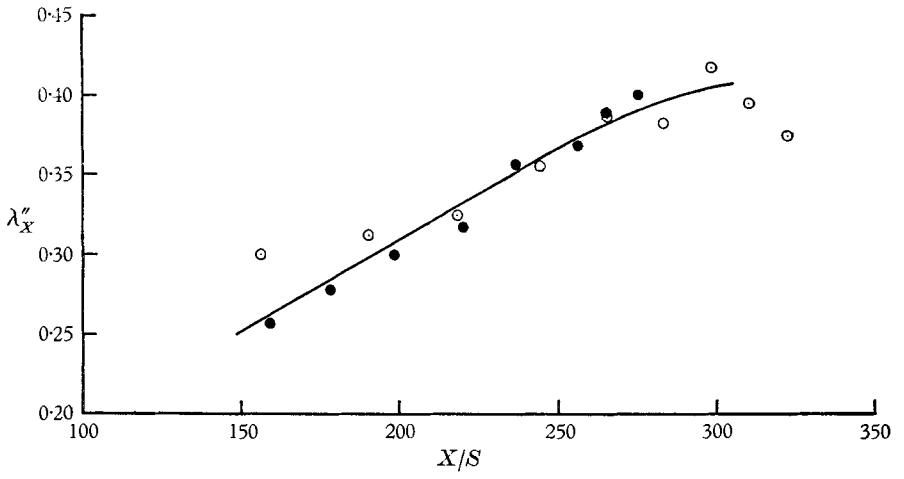

FIGURE 24. Microscale variation with effective distance from the grid. ●, Centre-line traverse; ⊙, lateral along gradient.

Figure 24 is the result obtained by replotting the microscale distributions of figures 23(*a*) and (23*b*) as functions of effective distance from the grid expressed in terms of the number of local rod spacings X/S. Values of λ_X measured at the greatest effective distances (figure 24) correspond to points at small Y/h in figure 23(*b*). Owing to experimental scatter, and the fact that the point farthest from the grid is also closest to the wall, the possibility of an asymptotic value of the microscale remains in question.

Summary of turbulence scales

Figures 23(*a*), 23(*b*), 25(*a*), and 25(*b*) summarize the results of microscale and integral scale values obtained from the correlations, time derivatives and energy spectra. Included on figure 23(*a*) is a comparison of the values of the longitudinal microscale calculated from the correlation coefficient $R_{uu}(r_X, 0, 0)$, $\lambda_X = 0{\cdot}48$ in., and from the time derivative, $\lambda_X = 0{\cdot}32$ in., both values corresponding to a centre-line location at X/h equal to 7·5. Of the two, the first is probably the more reliable. It is determined to within an estimated accuracy of $\pm 10\,\%$.

Sources of systematic error in scale values obtained from time derivatives include: finite wire length (Dryden, Schubauer, Mock & Skramstad 1937; Uberoi & Kovasznay 1953; Frenkiel 1954) and high-frequency response of both the R.M.S. Analyser (figure 4), and the differentiating circuit (figure 5). Since the flow is nearly homogeneous and the wire lengths roughly constant, corrections

would be quite uniform and alter the levels of the correlation coefficient distributions but effect little change in their shape.

A comparison of the longitudinal and lateral microscale distributions λ_X and λ_Y is given by figure 23(*b*). Both distributions show the same tendency of the scale magnitudes to increase with effective distance from the grid, X/S. They do not show local isotropy, i.e. $\lambda_X \neq \sqrt{2}\lambda_Y$.

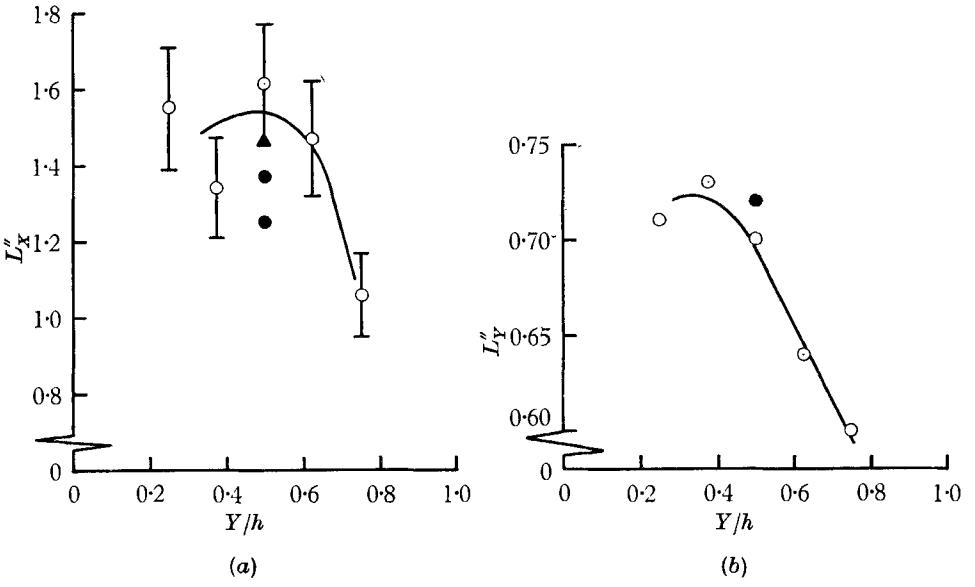

FIGURE 25. Lateral variation of integral scales: (*a*) longitudinal scale; (*b*) lateral scale.

(*a*) X/h: ⊙ 9·0, ● 7·5 — Obtained from spectra; ▲ 7·5 — Obtained from $R_{11}(r_X, 0, 0)$

(*b*) X/h: ⊙ 9·0, ● 7·5 — Obtained from $R_{uu}(0, r_Y, 0)$

Longitudinal integral scales are shown in figure 25(*a*). Two independently obtained values, from separate spectral measurements at $X/h = 7{\cdot}5$, give some indication of the probable error in the integral scales determined from spectra. Another check on these scales is provided by the single value determined from the longitudinal correlation coefficient $R_{uu}(r_X, 0, 0)$. Because of large scatter and the small number of determinations, the only conclusions possible are that the scale L_X is roughly one-tenth the size of the lateral dimension of the square test-section, and its magnitude tends to increase with effective distance from the grid. Lateral integral scales calculated from $R_{uu}(0, r_Y, 0)$ are shown in figure 25(*b*). These values also tend to increase with effective distance from the grid. The small difference in magnitude between the value of $X/h = 7{\cdot}5$ and $X/h = 9{\cdot}0$ is not significant. Comparing figures 25(*a*) and 25(*b*), L_X is found to be roughly twice L_Y.

4. Remarks

Initially, the present experiments were intended to give a quick look at the turbulence associated with a velocity field corresponding to a uniform mean shear. Work by other investigators, previously cited, established the possibility of generating the mean flow with linear velocity profile and provided an analytical background which facilitated design of the generating mechanism. No prior clues to the turbulence history were available. The experiments were pursued until the results indicated that the realized turbulent field lacked homogeneity of the scales and that the true nature of this field was partially obscured by extraneous effects.

Evaluation of the results leads to the conclusions that at sufficiently large distances from the generating grid and wall boundary layers, the turbulence intensities are maintained at uniform values by the constant mean shear, the turbulent shear-stress approaches an asymptotic value, the two-point space correlation coefficients and one-dimensional energy spectra attain self-preserving forms, and the turbulence scales over the limited extent of test-section available to measurement, increases with distance from the grid. Also the integral scales are roughly one-tenth the lateral dimensions of the square test-section or smaller.

The combined effects of persistence of grid-generated inhomogeneties, inadequate test-section length, wall boundary layer growth, and experimental uncertainty frustrate attempts to draw additional conclusions. It is the author's opinion that these effects can be either eliminated or adequately minimized and that the present results justify further attempts at realizing a homogeneous turbulent shear flow.

It is my pleasure to acknowledge the help and encouragement extended by my colleagues during this investigation. I hope that they will not be judged guilty by reason of association for any errors or omissions in its execution or results. This work was initiated by Prof. Stanley Corrsin, and carried out under his capable direction in the stimulating atmosphere of his laboratory. I am indebted to Dr Genevieve Comte-Bellot and Donald Kennedy for the daily discussions and voluntary assistance that help sustain one's enthusiasm. The initiative of Messrs William Hartman and Vascar Harris in the design, construction, and the collection of data is gratefully appreciated.

This work was supported by the Air Force AFOSR under contract AF 49(638)-1303.

REFERENCES

BATCHELOR, G. K. 1949 *Proc. Roy. Soc.* A, **195**, 513.

BATCHELOR, G. K. & PROUDMAN, I. 1956 *Phil. Trans.* A, **248**, 369.

BATCHELOR, G. K. & STEWART, R. W. 1950 *Quart. J. Mech. Appl. Math.* **3**, 1.

BOUSSINESQ, J. 1877 *Mem. prés. par div. sav., Paris*, **23**, 46.

BURGERS, J. M. & MITCHNER, M. 1953 *Proc. K. Akad. Wet. Amst.* B, **56**, 228, 343.

COLLIS, D. C. 1952 *Aero. Quart.* **4**, 93.

COMTE-BELLOT, G. 1965 *Publ. Scien. et Tech. du Ministere de l'Air*, no. 419, 1.

COMTE-BELLOT, G. & CORRSIN, S. 1965 The use of a contraction to improve the isotropy of grid-generated turbulence. Manuscript submitted for publication.

CORRSIN, S. 1957 *Naval Hydrodynamics Pub.* 515, *Nat. Acad. Sci./Nat. Res. Council, U.S. Gov't P.O.*, no. 373. Washington, D.C.

CORRSIN, S. 1963 *Handbuch der Physik*, **8/2**, 524.

CRAYA, A. 1958 *Publ. Scien. et Tech. du Ministere de l'Air*, no. 345, 1.

DEISSLER, R. G. 1961 *Phys. Fluids*, **10**, 1187.

DRYDEN, H. L. SCHUBAUER, G. B., MOCK, W. C. & SKRAMSTAD, H. K. 1937 *NACA Rep.* no. 581.

FOX, J. 1964 *Phys. Fluids*, **7**, 562.

FRENKIEL, F. N. 1954 *Aero. Quart.* **5**, 1.

GIBSON, M. M. 1963 *J. Fluid Mech.* **15**, 161.

GRANT, H. L. 1958 *J. Fluid Mech.* **4**, 149.

HINZE, J. O. 1959 *Turbulence.* New York: McGraw-Hill.

HUBBARD, P. G. 1957 *State Univ. of Iowa Studies in Engr. Bull.* **37**, 1.

VON KÁRMÁN, TH. 1937 *J. Aero. Sci.* **4**, no. 4, 131.

KOLPIN, M. A. 1964 *J. Fluid Mech.* **18**, 529.

LAUFER, J. 1951 *NACA Rep.* no. 1053, 15.

LIN, C. C. 1953 *Quart. Appl. Math.* **10**, 295.

LUMLEY, J. L. 1965 *Phys. Fluids*, **8**, 1056.

MCCARTHY, J. H. 1964 *J. Fluid Mech.* **19**, 491.

OWEN, D. R. & ZIENKIEWICZ, H. K. 1957 *J. Fluid Mech.* **2**, 521.

PASCERI, R. E. & FRIEDLANDER, S. K. 1960 *Can. J. Chem. Engr.* no. 212.

PRANDTL, L. 1925 *Z. angew. Math Mech.* **5**, 136.

REIS, F. B. 1952 Doctoral Dissertation, Dept. Math. M.I.T. 1.

ROSE, W. G. 1962 *J. Appl. Mech.* **29**, 615.

TAYLOR, G. I. 1915 *Phil. Trans.* A, **215**, 1.

TAYLOR, G. I. & BATCHELOR, G. K. 1949 *Quart. J. Mech. Appl. Math.* **2**, 1.

TOWNSEND, A. A. 1954 *Quart. J. Mech. Appl. Math.* **7**, 104.

TOWNSEND, A. A. 1956 *The Structure of Turbulent Shear Flow.* Cambridge University Press.

TRAUGOTT, S. C. 1958 *NACA TN*, no. 4125, 1.

UBEROI, M. S. & KOVASZNAY, L. S. G. 1953 *Quart. Appl. Math.* **10**, 375.